Pictorial Essay

Common patterns of perineural spread in head-neck squamous cell carcinoma identified on fluoro-deoxy-glucose positron emission tomography/computed tomography

Piyush Chandra, Nilendu Purandare, Sneha Shah, Archi Agrawal, Venkatesh Rangarajan

Department of Nuclear Medicine and Molecular Imaging, Tata Memorial Hospital, Mumbai, Maharashtra, India

ABSTRACT

Perineural spread in HNSCC is associated with dismal prognosis and decreased overall survival. Clinical diagnosis of this relatively asymptomatic entity is usually delayed and made incidentally on imaging. MRI is gold standard imaging for early diagnosing of this condition owing to its excellent anatomic resolution. With the ever increasing use of PET/CT in commonly encountered cancer such as HNSCC for staging and re-staging, observing perineural spread on PET/CT is not infrequent. Through this pictorial essay we demonstrate the common patterns of perineural spread in HNSCC on PET/CT with the aim of improving reporting accuracy across readers.

Keywords: Fluoro-deoxy-glucose, head-neck, magnetic resonance, perineural spread, positron emission tomography/computed tomography, squamous cell carcinomas

INTRODUCTION

Malignancies of the head/neck (HN), especially the squamous cell carcinomas (SCCs) cancers arising in the oral cavity, are common in India and constitute a major public health problem. Most common ways of the spread for carcinomas in HN is by lymphatic route and in few cases hematogenous. Some tumors however have a propensity to spread to a distant site through perineural route. The exact reason for this phenomenon is presently unclear; probably the nerve appears to form a natural channel and conduit of least resistance along the otherwise "difficult-to-traverse" complex HN anatomy.

Perineural spread (PNS) in HN malignancies implies a grave prognosis with poor event-free and overall survival in patients with SCC compared to those without it.[1-3] PNS is more often a radiological diagnosis as many patients are clinically asymptomatic. This important prognostic finding, however, is frequently under-reported with most patients identified on retrospective review of radiographic images than on the initial scans.[4] With increasing use of 2-fluoro-deoxy-glucose (FDG) positron emission tomography with contrast-enhanced computed tomography (PET/CECT) in the evaluation of HN malignancy for staging, re-staging, and response evaluation, the observation of PNS being noticed early on PET/computed tomography (PET/CT) is not uncommon. The aim of this pictorial assay is to increase awareness of this entity by demonstrating the various patterns of PNS in HN cancers seen on PET/CT.

CLINICAL PRESENTATION

Increased risk of PNS in HN cancers is seen in males, increasing tumor size, mid-face location, recurrent disease setting, and poorly differentiated tumors.[5] The clinical diagnosis of

Address for correspondence:
Dr. Venkatesh Rangarajan, Department of Nuclear Medicine and Molecular Imaging, Tata Memorial Hospital, E. Borges Road, Parel, Mumbai - 400 012, Maharashtra, India.
E-mail: drvrangarajan@gmail.com

Access this article online

Quick Response Code:

Website: www.ijnm.in

DOI: 10.4103/0972-3919.190798

How to cite this article: Chandra P, Purandare N, Shah S, Agrawal A, Rangarajan V. Common patterns of perineural spread in head-neck squamous cell carcinoma identified on fluoro-deoxy-glucose positron emission tomography/computed tomography. Indian J Nucl Med 2016;31:274-9.

PNS is often challenging (delayed/missed) as majority of the patients may be clinically asymptomatic for the same. The role of imaging, hence, in this condition is crucial. Imaging will help identify subsets of patients who would need alterations in surgical plan and/or adjuvant therapies (chemotherapy/radiation). The common histological subtypes associated with PNS (in decreasing order of frequency) are SCCs, adenoid cystic carcinoma, mucoepidermoid carcinoma, skin cancers, and lymphoma.

Pathological anatomy of perineural spread

Commonly involved cranial nerves in PNS are mandibular division of trigeminal nerve (V3), maxillary nerve (V2), facial nerve (VII), and hypoglossal nerve (XII) due to their long extensive course in the HN region. The anatomical knowledge of the course of these nerves is essential in the clinicoradiological diagnosis of PNI [Table 1].[6] V2 nerve is usually involved by direct invasion though tumors in the upper lip or malar surface and tumors of nasopharynx or palate though the palatine nerves [Figure 1]. V3 nerve is usually involved by the tumors in the lower lip/alveolus spreading through inferior alveolar nerve, or parotid/infratemporal fossa tumors spreading via the auriculotemporal branch [Figures 2-6] PNS along facial (VII) nerve is usually involved by tumors of parotid glands, extending into the stylomastoid foramen and temporal bone. PNS along hypoglossal nerve (XII) involvement is seen with tumors of the tongue base and nasopharyngeal tumors [Figures 7 and 8]. Due to close proximity of the branches of these nerves, simultaneous multiple cranial nerve involvement in is not uncommon [Figure 5].

Magnetic resonance imaging in diagnosis of perineural spread

PNS is best and earliest detected with a contrast-enhanced T1-fat suppressed magnetic resonance (MR) sequences. Due

Table 1: Commonly involved cranial nerve and their course in head/neck

Cranial nerve	Course
Maxillary (V2)	Arises from the trigeminal ganglion, courses anteriorly in lateral wall of cavernous sinus and passes through foramen rotendum, through the upper part of pterygopalatine fossa, then enters orbit through inferior orbital fissure and exits orbit through infra-orbital foramen as infraorbital nerve
Mandibular (V3)	Arises from the trigeminal ganglion, exits the skull through foramen ovale, then enters the infra-temporal fossa supplying the muscles of mastication, then dividing into anterior trunk (lingual nerve) and posterior trunk (inferior alveolar nerve)
Facial (VII)	Emerges from the brain stem, and continues into the internal acoustic meatus, then runs posterior to geniculate ganglion, into the tympanic segment in the medial wall of middle ear cavity, makes a bend exiting the skull though the stylomastoid foramen, passes between post belly of digastric and stylohyoid to lie between the deep and superficial lobes of parotid finally dividing into 5 main braches supplying facial muscles
Hypoglossal (XII)	Originating from the medulla, nerve enters the hypoglossal canal, passes obliquely downwards between the internal jugular and internal carotid artery, then runs forward, crossing the loop at the origin of lingual artery, then passing superficial to the hyoglossus muscle, and forward into the tongue supplying all the muscles except palatoglossus

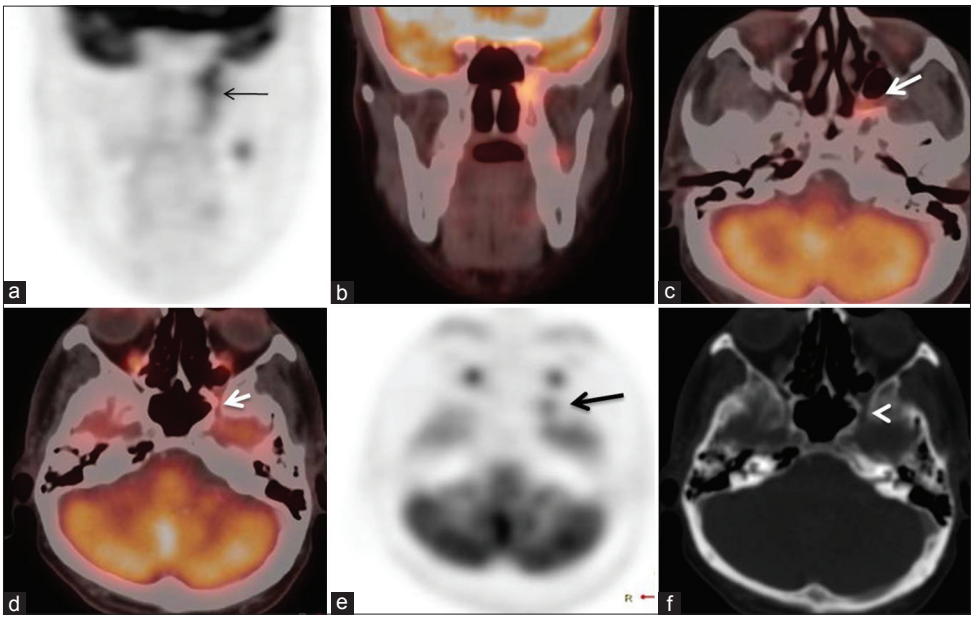

Figure 1: Perineural spread along maxillary (V2) nerve: 49-year-old male, known case of carcinoma soft palate, received radiotherapy 1 year back, now presenting with pain in the left side of face. Linear fluoro-deoxy-glucose uptake noted in the region of the left pterygomaxillary fissure on coronal fluoro-deoxy-glucose positron emission tomography (a) and coronal fused fluoro-deoxy-glucose positron emission tomography/computed tomography (b) images. Transaxial fused positron emission tomography/computed tomography images (c and d) fluoro-deoxy-glucose uptake extending into the widened left pterygopalatine fossa (long white arrow) and then into the left foramen rotundum (short bold white arrow). The asymmetric uptake in the left foramen rotundum (black arrow) is noted on transaxial positron emission tomography images (e). Widened left foramen rotundum (white arrowhead) is noted on transaxial computed tomography images (f)

to break in the blood-nerve barrier caused by the tumor, the enhancement of the nerve precedes the nerve enlargement. Further proliferation of the tumor leads to the replacement of the perineural fat and widening/erosion of foramen in skull bases. The nerve invasion by tumor may be seen as a continuous nerve enhancement or skip lesion at a distant site in nerve probably through perineural lymphatics. Indirect features of nerve involvement like muscle denervation seen as hyperintense T2 signals in the muscle secondary to edema can supplement the MR diagnosis of PNS [Figure 8].[7]

Positron emission tomography/computed tomography for diagnosis of perineural spread

The use of PET/CT in HNSCC is increasing. Superior diagnostic accuracy PET/CT over conventional morphological imaging has been established, especially for evaluating nodal and distant metastasis, to assess disease recurrence, assessing response to curative chemoradiotherapy or neo-adjuvant chemotherapy, and predicting treatment outcomes.[8] Detection of PNS of tumor on PET/CECT is not uncommon. The accuracy of PNS detection on PET/CT is lower than MR, owing to lower anatomical resolution, image artifacts, and higher incidence of false positive/false negative interpretations. It can, however, compliment MR in diagnosis of PNS or may be useful where MR is contra-indicated such as claustrophobia and renal insufficiency. Certain clues to image interpretation may help increase the reporting accuracy of PET/CECT for diagnosis of PNS in HNSCC [Table 2]. On PET/CT image, one should look for asymmetric increased linear/curvilinear FDG uptake in the region of nerve course (infratemporal fossa, pterygopalatine fossa, or nerve foramen) which may be contiguous or discontiguous with the primary/recurrent tumor [Figures 1-4]. It is important to assess maximum intensity projection and all the three planes of the PET images. On CT images, one must look for any enhancement along the nerve course, loss of fat planes with soft tissues adjacent to the nerves, and widening/erosion of neural foramina [Figures 1 and 3]. Use of diagnostic quality CT, i.e., contrast-enhanced, high mA with thin bone window CT sections in the PET/CT protocol is of prime importance in diagnosing PNS in HNSCC.[9] CT reconstruction parameters used at our institute for HN region includes slice thickness of 0.67 mm, field of view of 250 mm, window - 35 × 350, increment - 0.33 mm, and matrix of 512. About 80 ml of low osmolar nonionic intravenous contrast is administered in all patients at a rate of 1.8 ml/s and scan delay is usually about 50–60 s.

Care should be taken to avoid frequent false negative/false positive interpretations on PET/CECT in HNSCC cases.

Table 2: Key features on PET/CECT in evaluating peri-neural spread

PET
• Focal/linear/curvilinear and asymmetric tracer uptake anywhere along the course of V2, V3, VII and XII nerve
• Uptake may or may not be in contiguity with primary disease
• Uptake may be heterogeneous/low grade or absent
CECT
• Enhancement, soft tissue mass/fat replacement in the neural foramina/fissures
• Widening/lytic erosion of the neural foramina/fissures
• Comparing involved neural foramen/fissures with the contralateral side

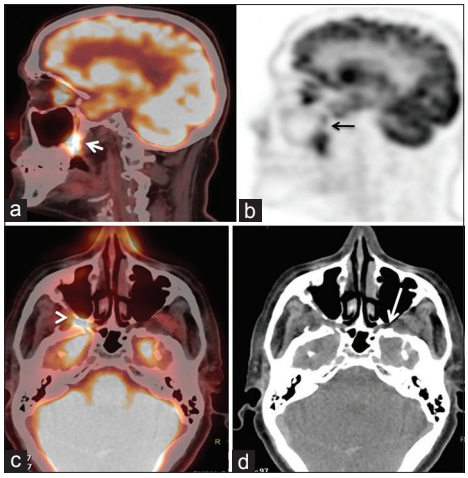

Figure 2: Perineural spread along maxillary (V2) nerve: 63-year-old male, treated case of Ca right buccal mucosa 5 years back, presenting with trismus and hypoesthesia of the right side of face. Sagittal fused positron emission tomography/computed tomography (a) Fluoro-deoxy-glucose uptake in the disease in the right retromolar trigone (white arrow). Sagittal positron emission tomography (b) linear fluoro-deoxy-glucose uptake extending from receptor-mediated transport into pterygopalatine fossa and inferior orbital fissure (black arrow). Transaxial fused positron emission tomography/computed tomography (c) shows increased asymmetric fluoro-deoxy-glucose uptake in the right pterygopalatine fossa (white arrowhead). Transaxial computed tomography (d) images show widened pterygopalatine fossa with loss of fat and enhancement within, compared to the normal pterygopalatine fossa on the left side (white arrow)

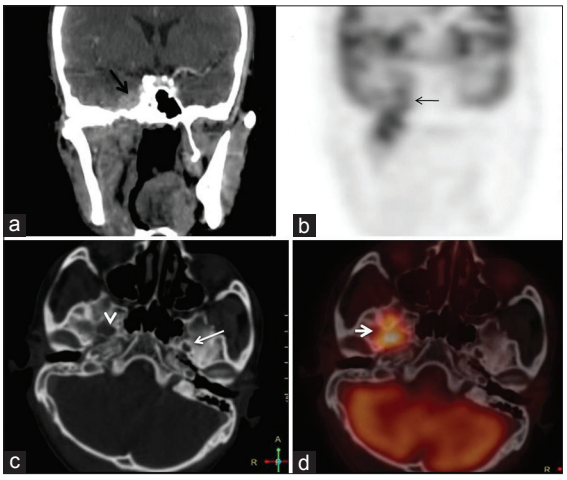

Figure 3: Perineural spread along mandibular (V3) nerve: 35-year-old male, treated case of Ca right lower Guillain–Barré syndrome, now presenting with deep-seated headache. Transaxial computed tomography (a) enhancing soft tissue mass in the right infratemporal fossa extending intracranially into the middle cranial fossa (black arrow). Correlative coronal positron emission tomography (b) linear fluoro-deoxy-glucose uptake extending from infratemporal fossa up to the middle cranial fossa (black arrow). Transaxial computed tomography (c) widened right foramen ovale (white arrowhead) compared to the normal foramen on the left (long white arrow). Transaxial fused positron emission tomography/computed tomography (d) asymmetric increased fluoro-deoxy-glucose uptake in the soft tissue mass in the right foramen ovale (small white arrow)

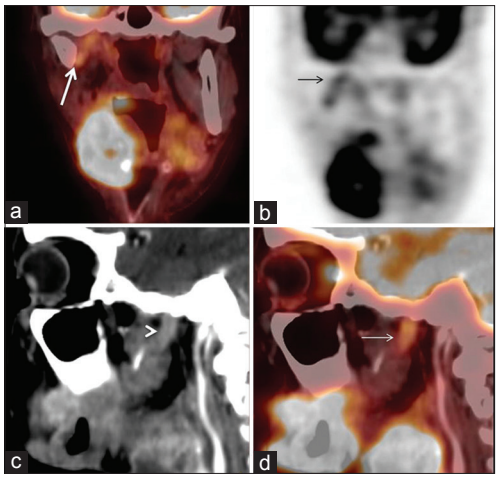

Figure 4: Perineural spread along mandibular (V3) nerve: 47-year-old male, operated case of the right buccal mucosa and received adjuvant chemoradiotherapy, after short disease-free interval of 4 months, presented with recurrent lesion over right buccal mucosa. Coronal fluoro-deoxy-glucose (a) and fused positron emission tomography/computed tomography (b) images show recurrent soft tissue mass in the right oral cavity, extending into the floor of mouth, with linear fluoro-deoxy-glucose uptake along the right masseteric space extending into the right foramen ovale (black arrow). Sagittal computed tomography (c) shows enhancing soft tissue mass in the right infratemporal fossa along the V nerve course (white arrowhead). Sagittal fused positron emission tomography/computed tomography (d) shows fluoro-deoxy-glucose uptake along the enhancing soft tissue mass along the V nerve course extending into the base of skull (white arrow)

The uptake intensity along the nerve course may be subtle leading to false negative scan, probably attributed to tumor biology (less uptake in salivary gland and necrotic neoplasm), improper PET/CT image co-registration, partial volume effect for smaller lesions (<1 cm), or high adjacent background activity in brain [Figure 6]. False positive scans can be seen in setting such as postradiotherapy/postoperative inflammation, asymmetric physiological FDG uptake in the facial muscles, hyper-enhancing primary neural tumors (schwannoma/meningiomas) [Figure 9], invasive fungal infections, and dental abscesses. Careful assessment of the patients' history, clinical features, and assessment of correlative imaging can help avoid such pitfalls.[10-13]

Positron emission tomography/magnetic resonance for detection of perineural spread

Feasibility of clinical PET/MR for imaging HN tumors has been suggested by few studies.[14,15] In addition to providing significantly less radiation exposure to the patient, this modality appears to have a higher spatial resolution, due to reduced partial volume effects and lesser chance of signal loss that is seen with small structures in HN.[14] This will translate into higher target to background contrast, further enhancing detection of PNS in HN SCC compared to that provided by the existing PET/CT systems.

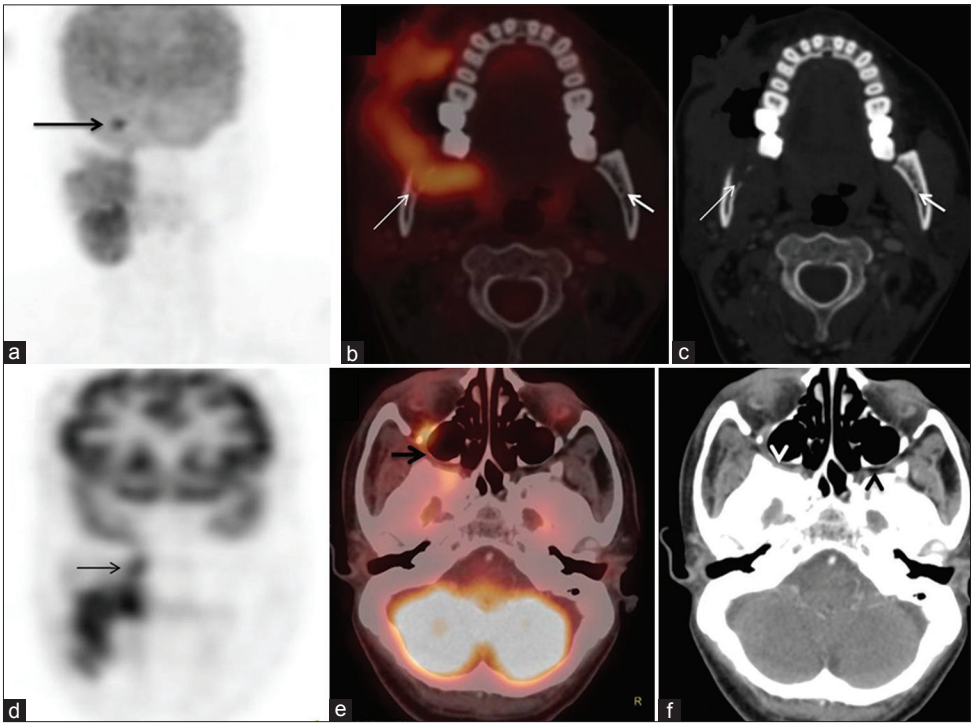

Figure 5: Perineural spread along V2 and V3 nerve: 33-year-old male, Ca right buccal mucosa presenting with trismus. Coronal fluoro-deoxy-glucose positron emission tomography (a) uptake in buccal mucosa, infratemporal fossa and focal uptake in the right orbit (black arrow). Transaxial positron emission tomography/computed tomography (b) fluoro-deoxy-glucose avid mass in the right lower alveolus, extending into widened inferior alveolar canal (long white arrow) and normal left alveolar canal on transaxial computed tomography (c) (short white arrow). Coronal fluoro-deoxy-glucose positron emission tomography (d) linear uptake along pterygopalatine fossa (thin black arrow). Transaxial positron emission tomography/computed tomography (e) asymmetric curvilinear uptake in the right inferior orbital fissure (short black arrow) seen as fat replacement on transaxial computed tomography (f) (white arrowhead), compared to normal left (black arrowhead)

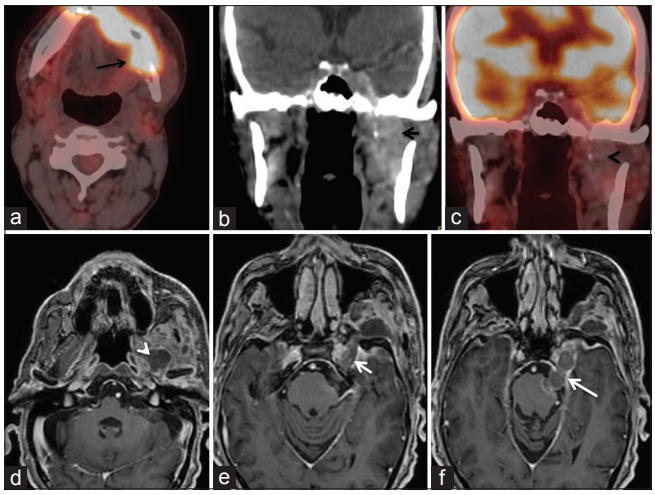

Figure 6: Perineural spread along V3 nerve: 57-year-old male, with Ca left lower alveolus, presented with trismus. Transaxial fluoro-deoxy-glucose positron emission tomography/computed tomography (a) uptake in soft tissue mass in the left lower alveolus widening and eroding the inferior alveolar canal (long black arrow). Coronal computed tomography (b) enhancing soft tissue mass extending from the infratemporal fossa intracranially through the widened foramen ovale (short black arrow) and showing no significant fluoro-deoxy-glucose uptake in the coronal fused fluoro-deoxy-glucose positron emission tomography computed tomography (black arrowhead) (c). Serial sections of axial postcontrast magnetic resonance sequences (d-f) reveals mass in the left masticator space extending cranially along the mandibular nerve (white arrowhead), trigeminal ganglion (short white arrow) up to the lateral aspect of pons (long white arrow)

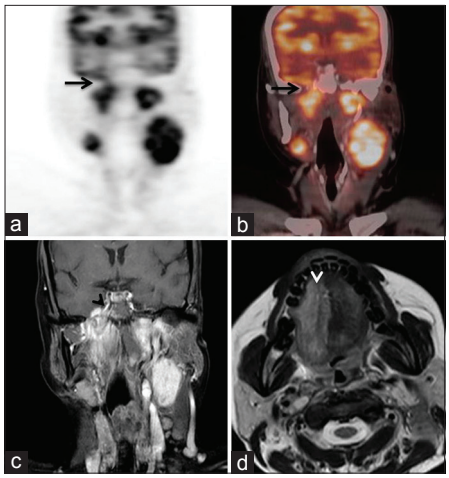

Figure 8: Perineural spread along the hypoglossal nerve (XII): 43-year-old female, with Ca nasopharynx. Staging positron emission tomography/computed tomography shows fluoro-deoxy-glucose uptake in the soft tissue mass in the bilateral nasopharynx and bilateral enlarged cervical nodes on coronal positron emission tomography (a) and fused positron emission tomography/computed tomography images (b) with linear asymmetric increased uptake along the right hypoglossal canal (black arrows). Correlative coronal T1-weighted fat suppressed postcontrast magnetic resonance image (c) enhancing mass in the right nasopharynx extending into hypoglossal canal (black arrowhead) causing denervation of the ipsilateral half of tongue seen as increased signal on transaxial T2-weighted magnetic resonance image (white arrowhead, d)

CONCLUSION

PNS in HN malignancies is uncommon but a dreadful event. Clinical presentation is usually delayed due to lack of symptoms and diagnosis is very often confirmed on imaging. MR imaging is the gold standard for identification of PNS and outperforms the diagnostic accuracy of CECT or PET/CT for this indication. With recent exponential increase in the use of PET/CT in HNSCC, identifying clinically occult PNS on PET/CT is not uncommon, thereby complementing MR in diagnosis and potentially obviating further diagnostic interventions. A precise knowledge of clinical presentation, regional anatomy, and correlative imaging is, however, a prerequisite and which may help the nuclear medicine physician in avoiding image misinterpretations. This would improve the reporting accuracy of PET/CT and along with recent advances in technology such as PET/MR would together promote molecular imaging toward being a "standard of care" in diagnostic evaluation of HN malignancies.

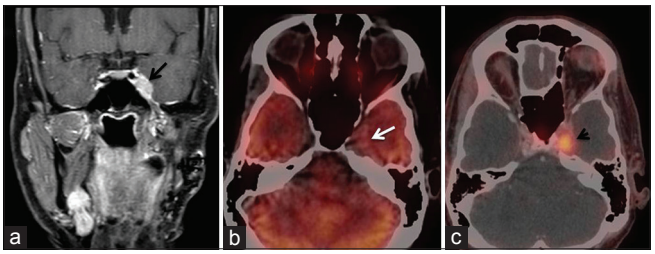

Figure 7: Left parasellar meningioma, mimicking perineural spread: 44-year-old male, operated case of Ca left parotid presenting with headache. Coronal T1-weighted magnetic resonance with contrast (a) ill-defined enhancing mass in the left parasellar region (black arrow) and along the mandibular division of V nerve in the suspicious for perineural spread. Transaxial fluoro-deoxy-glucose positron emission tomography/computed tomography (b) no significant uptake in the enhancing mass in the left parasellar region (white arrow). Transaxial positron emission tomography/computed tomography using ^{68}Ga-DOTA-NOC (c) showed uptake in the left parasellar mass. Clinicoradiological features favored of nerve sheath tumor, likely meningioma and patient improved with symptomatic mediations on follow-up

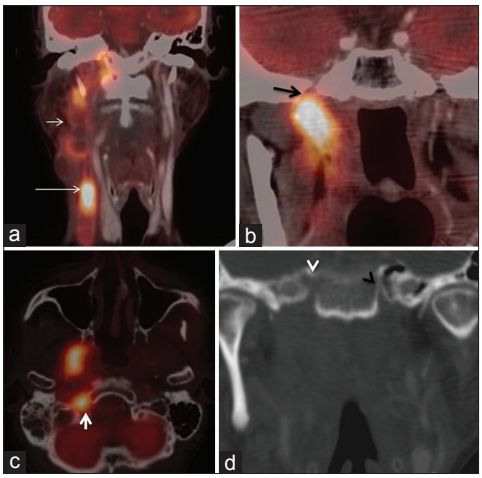

Figure 9: Perineural spread along the hypoglossal nerve (XII): 62-year-old male, operated case of Ca left buccal mucosa, complained of right neck swelling. Coronal fluoro-deoxy-glucose positron emission tomography/computed tomography (a) uptake in the tumor thrombus in the right internal jugular vein and in necrotic right level II/III nodes. Coronal fluoro-deoxy-glucose positron emission tomography/computed tomography (b) uptake in the soft tissue mass in the right masseteric space extending into the foramen ovale. Transaxial fluoro-deoxy-glucose positron emission tomography/computed tomography (c) uptake in the soft tissue mass in the posterior base of skull, eroding the right jugular and hypoglossal canal (short white arrow). Coronal computed tomography (d) widening and erosion of the right hypoglossal canal (white arrowhead), compared to the normal left (black arrowhead)

Financial support and sponsorship

Nil.

Conflicts of interest

There are no conflicts of interest.

REFERENCES

1. Liebig C, Ayala G, Wilks JA, Berger DH, Albo D. Perineural invasion in cancer: A review of the literature. Cancer 2009;115:3379-91.
2. Meng FY, Ko JY, Lou PJ, Wang CP, Yang TL, Chang CH, *et al*. The determining risk factors for treatment outcomes in patients with squamous cell carcinoma of the hard palate. Ann Surg Oncol 2012;19:2003-10.
3. Majoie CB, Hulsmans FJ, Verbeeten B Jr., Castelyns JA, Oldenburger F, Schouwenburg PF, *et al*. Perineural tumor extension along the trigeminal nerve: Magnetic resonance imaging findings. Eur J Radiol 1997;24:191-205.
4. Lee KJ, Abemayor E, Sayre J, Bhuta S, Kirsch C. Determination of perineural invasion preoperatively on radiographic images. Otolaryngol Head Neck Surg 2008;139:275-80.
5. Balamucki CJ, Mancuso AA, Amdur RJ, Kirwan JM, Morris CG, Flowers FP, *et al*. Skin carcinoma of the head and neck with perineural invasion. Am J Otolaryngol 2012;33:447-54.
6. Sinnatamby, Chummy S, R. J Last. Last's Anatomy. 12th ed. Edinburgh: Churchill Livingstone/Elsevier; 2011.
7. Ong CK, Chong VF. Imaging of perineural spread in head and neck tumours. Cancer Imaging 2010;10:S92-8.
8. Evangelista L, Cervino AR, Chondrogiannis S, Marzola MC, Maffione AM, Colletti PM, *et al*. Comparison between anatomical cross-sectional imaging and 18F-FDG PET/CT in the staging, restaging, treatment response, and long-term surveillance of squamous cell head and neck cancer: A systematic literature overview. Nucl Med Commun 2014;35:123-34.
9. Paes FM, Singer AD, Checkver AN, Palmquist RA, De La Vega G, Sidani C. Perineural spread in head and neck malignancies: Clinical significance and evaluation with 18F-FDG PET/CT. Radiographics 2013;33:1717-36.
10. Blodgett TM, Fukui MB, Snyderman CH, Branstetter BF 4th, McCook BM, Townsend DW, *et al*. Combined PET-CT in the head and neck: Part 1. Physiologic, altered physiologic, and artifactual FDG uptake. Radiographics 2005;25:897-912.
11. Fukui MB, Blodgett TM, Snyderman CH, Johnson JJ, Myers EN, Townsend DW, *et al*. Combined PET-CT in the head and neck: Part 2. Diagnostic uses and pitfalls of oncologic imaging. Radiographics 2005;25:913-30.
12. Wong RJ, Lin DT, Schöder H, Patel SG, Gonen M, Wolden S, *et al*. Diagnostic and prognostic value of [(18) F]fluorodeoxyglucose positron emission tomography for recurrent head and neck squamous cell carcinoma. J Clin Oncol 2002;20:4199-208.
13. Gandhi D, Gujar S, Mukherji SK. Magnetic resonance imaging of perineural spread of head and neck malignancies. Top Magn Reson Imaging 2004;15:79-85.
14. Platzek I, Beuthien-Baumann B, Schneider M, Gudziol V, Langner J, Schramm G, *et al*. PET/MRI in head and neck cancer: Initial experience. Eur J Nucl Med Mol Imaging 2013;40:6-11.
15. Schaarschmidt BM, Heusch P, Buchbender C, Ruhlmann M, Bergmann C, Ruhlmann V, e*t al*. Locoregional tumour evaluation of squamous cell carcinoma in the head and neck area: A comparison between MRI, PET/CT and integrated PET/MRI. Eur J Nucl Med Mol Imaging 2016;43:92-102.